Isoscalar E0, E1, and E2 strength in ^{44}Ca

J. Button, Y.-W. Lui, D. H. Youngblood, X. Chen, G. Bonasera, and S. Shlomo

Phys. Rev. C **96**, 054330 — Published 29 November 2017

DOI: 10.1103/PhysRevC.96.054330

Isoscalar E0, E1, and E2 strength in ^{44}Ca

J. Button[1], Y. -W. Lui[1], D. H. Youngblood[1], X. Chen[2], G. Bonasera[1], and S. Shlomo[1]

[1]Cyclotron Institute, Texas A&M University, College Station, Texas 77843, USA.
[2]Department of Radiation Oncology, Medical College of Wisconsin, Milwaukee, Wisconsin 53226, USA

Isoscalar giant resonances in ^{44}Ca have been studied with inelastic scattering of 240 MeV α particles at small angles including 0°. A majority of the Energy Weighted Sum Rule was identified for E0 and E2 (≈70%), and nearly half was identified for E1. The strength distributions are compared with the predictions from Hartree-Fock based Random Phase Approximation calculations with the KDE0v1 Skyrme-type interaction. The GMR energy moments for ^{40,44,48}Ca increase with mass, contrary to what would be expected with a negative symmetry energy, K_τ.

PACS numbers: 25.55.Ci, 24.30.Cz, 27.60.+j

I. INTRODUCTION

The Isoscalar Giant Monopole Resonances (ISGMRs) in ^{40}Ca and ^{48}Ca have been studied [1,2], and contrary to expectations that the ISGMR energy in ^{48}Ca would be lower than in ^{40}Ca (Giant Resonance (GR) energies generally go roughly as $A^{-1/3}$ in the simplest models and the negative K_{sym} term in the Leptodermous expansion [3] leads to a decreasing energy with increasing A) the energy of the ISGMR in ^{48}Ca is higher than in ^{40}Ca. Anders et al. [4] investigated this at length using a number of interactions in HF-RPA calculations but were unable to reproduce this behavior. We have studied the isoscalar giant resonances in ^{44}Ca in hopes of shedding some light

on this and to further explore the behavior of the isoscalar dipole and quadrupole resonances in the Ca isotopes.

In this paper we report E0, E1, and E2 multipole strength distributions obtained for ^{44}Ca and compare the experimental distributions with those obtained for ^{40}Ca and ^{48}Ca and with theoretical predictions from the results of Hartree-Fock (HF) based Random Phase Approximation (RPA) calculations [5] with the KDE0v1 Skyrme-type effective interaction [2,6].

II. EXPERIMENTAL PROCEDURE

The experimental technique has been described thoroughly in Refs. [7,8] and is summarized briefly below. Beams of 240 MeV α particles from the Texas A&M K500 superconducting cyclotron bombarded a self-supporting ^{44}Ca foil of 5.0 mg/cm^2 enriched to more than 95% in the desired isotope, located in the target chamber of the multipole-dipole-multipole (MDM) spectrometer. The target thickness was measured by weighing and checked by measuring the energy loss of the 240 MeV α beam in the ^{44}Ca target.

Data were taken with the MDM spectrometer at 0.0° (0.0° < θ < 2.0°) and at 4.0° (2.0° < θ < 6.0°). The details of the MDM spectrometer design and operation can be found in Ref. [9]. The focal plane detector (described thoroughly in Refs. [10,11]) measured position and angle in the scattering plane, covering $E_x \approx$ 8 MeV to E_x > 55 MeV (depending on scattering angle). Sample spectra obtained for ^{44}Ca are shown in Figure 1.

.

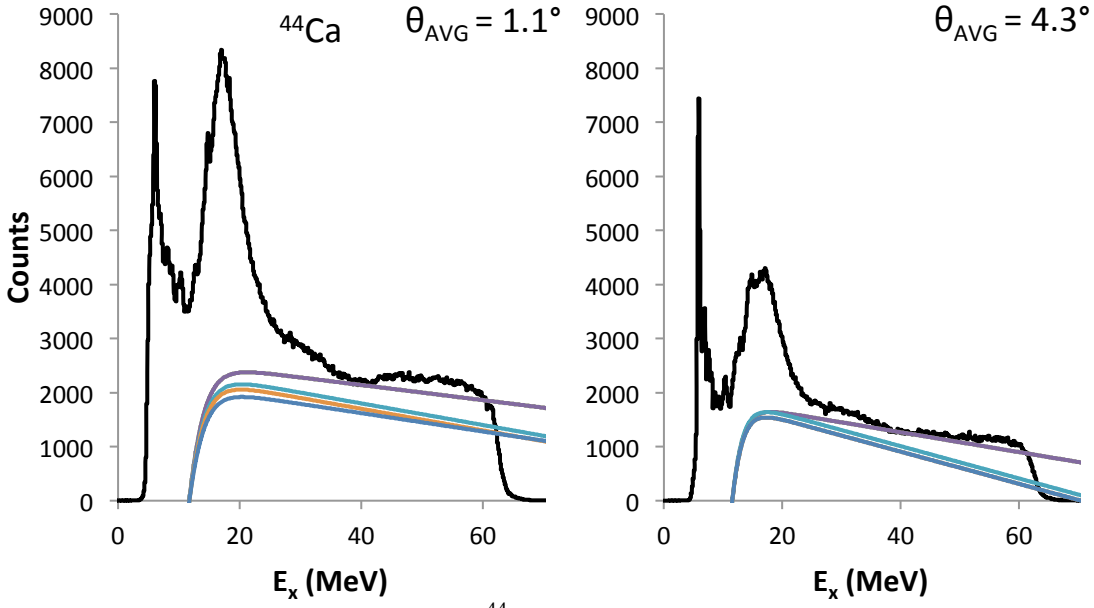

Figure 1. Inelastic α spectra obtained for ^{44}Ca are shown. The lines are examples of continua chosen for analyses.

III. MULTIPOLE ANALYSIS

Single-folding Distorted Wave Born Approximation (DWBA) calculations with optical model potentials (as described in Refs. [7,8,12]) were carried out with PTOLEMY [13]. Optical model parameters obtained for 240 MeV α scattering on ^{48}Ca [2] were used and are shown in Table I.

Table I. Optical Model and Fermi parameters [14] used in DWBA calculations are listed, R_{c_0} is the Coulomb radius parameter.

V (MeV)	W (MeV)	R_i (fm)	a_i (fm)	R_{c_0} (fm)	c(fm)	a(fm)
47.392	31.495	4.907	0.677	4.912	3.784	.523

Calculations were performed with the Fermi form for the mass distribution [15,16], $\rho(r) = \rho_0 \left[1 + e^{\frac{r-c}{a}}\right]^{-1}$, with c and a shown in Table I [14]. The calculations for the transition densities, sum rules, and DWBA calculations were discussed thoroughly in Refs. [7,8,12,17].

The inelastic α spectra obtained are each divided into a peak and continuum background. The details of the continuum background and its effect on experimental uncertainties are discussed in Ref. [18]. Typical choices for the continuum can be seen in Figure 1. The peak and continuum cross-sections are then divided into bins by excitation energy. A description for how to obtain the multipole components for each experimental bin can be found in Ref. [18]. The experimental and calculated angular distributions are illustrated in Figure 2 for selected energy bins in the GR region.

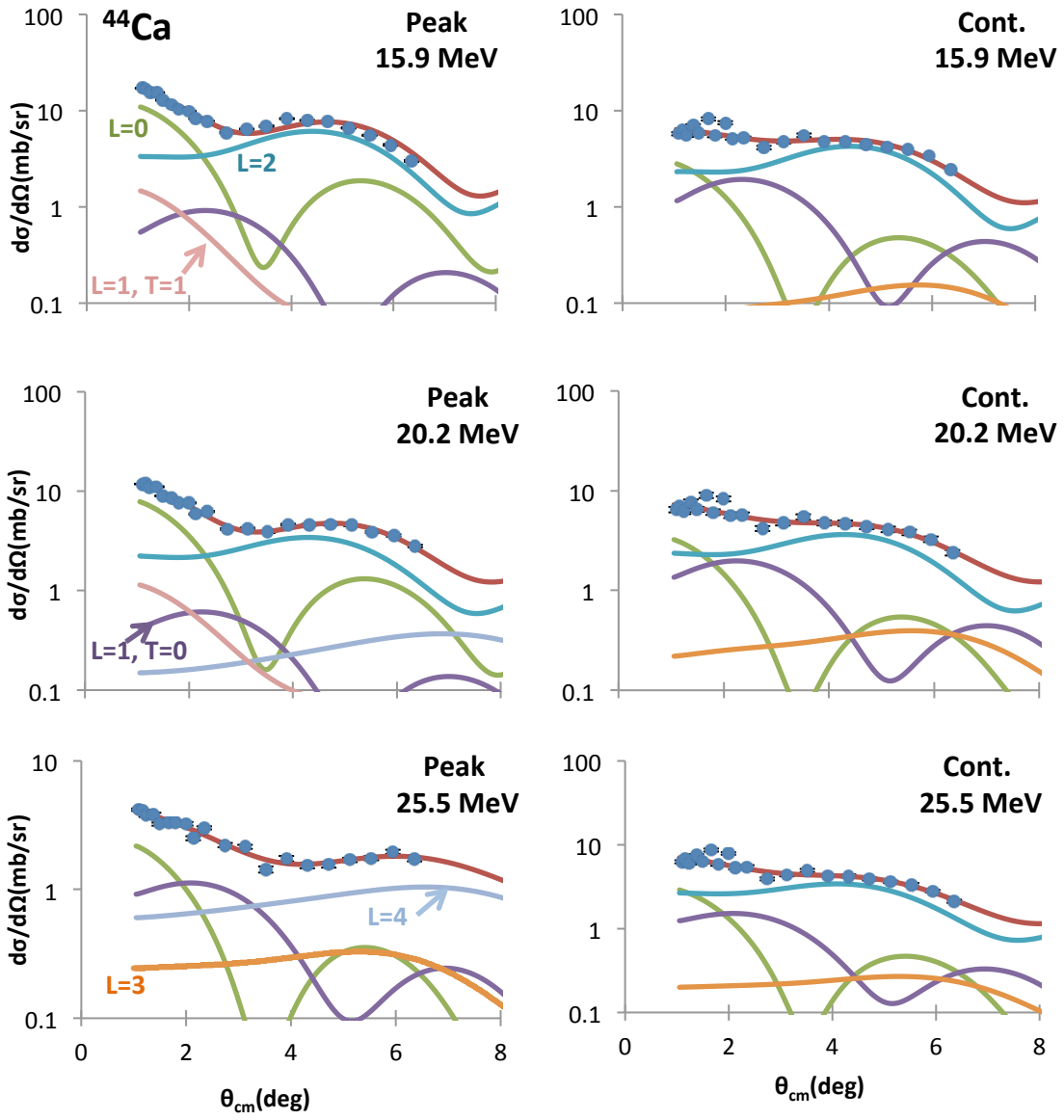

Figure 2. The angular distributions of the ^{44}Ca cross sections for three excitation ranges of the GR peak and the continuum are plotted vs. center-of-mass scattering angle. Each bin is 480 keV wide and the average energies for each bin are shown. The lines through the data points indicate the multipole fits. The contributions of each multipole are shown. The statistical errors are smaller than the data points.

IV. DESCRIPTION OF MICROSCOPIC CALCULATIONS

Microscopic mean-field based Random Phase Approximation (RPA) theory provides a description of collective states in nuclei [19,20]. A description of the spherical HF-based RPA calculations of the strength functions and centroid energies of the isoscalar (T=0) giant resonances in nuclei can be found in Ref. [21] .

The fully self-consistent mean field calculation of the strength or response function uses an effective two-nucleon interaction which is obtained from a fit to the ground states properties of nuclei. The effective interaction determines the HF mean-field. The KDE0v1 Skyrme-type effective interaction was used because, in an external test of 240 Skyrme-type effective interactions [22,23], the KDE0v1 was the only one to pass constraints relating to experimental data on properties of nuclear matter and nuclei. For a more thorough discussion of the microscopic calculations, please see Ref. [2].

The appropriate experimental excitation energy ranges were used: 9-40 MeV for the ISGMR and Isoscalar Giant Quadrupole Resonance (ISGQR), 9-20 MeV for the low-component of the Isoscalar Giant Dipole Resonance (ISGDR), and 20-36 MeV for the high-component of the ISGDR. The calculated distributions are shown superimposed on the experimental results in Figure 3. The smearing width (Γ) for the calculated distributions for the E0-E2 multipoles are shown in Table 2. The energy moments are included in Tables III and V. The theoretical strengths are calculated over a range of 0 to 100 MeV and contain 100% of the EWSR for E0-E2.

Table II. Smearing widths for the calculated distributions are shown.

	E0	E1	E2
Γ (MeV)	6.5	13.0	10.0

IV. DISCUSSION

The E0-E2 multipole distributions obtained for ^{44}Ca are shown in Figure 3. A two-peak fit is shown for the E1 distribution, and single Gaussian fits are shown for E0 and E2. The parameters for the experimental distributions are shown in Table III. The parameters for the Gaussian fits and for the moments of the calculated distributions are shown in Table IV and Table V respectively. Due to the limited angular range of the data, E3 and E4 or higher multipole strength could not be distinguished unambiguously. The highest multipole included in the fits is E4, and the "E3 +E4" distribution shown in Figure 3 is the sum of all the multipoles $L \geq 3$.

The theoretical energy moments and strengths in Tables III and V are for the experimental energy ranges (E0: $9 \leq E_x \leq 40$ MeV , E1 low range: $9 \leq E_x \leq 20$ MeV, E1 high range: $20 \leq E_x \leq 40$ MeV, and E2: $9 \leq E_x \leq 40$ MeV).

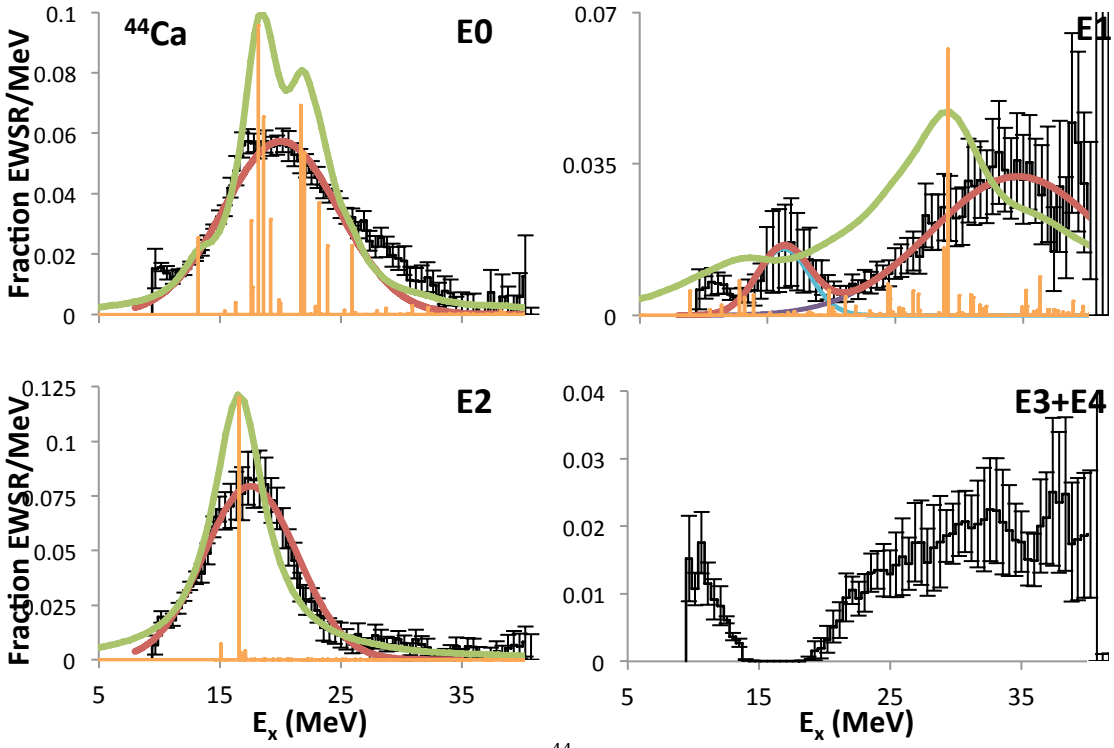

Figure 3. Strength distributions obtained for ^{44}Ca are shown by the histograms. Error bars represent the uncertainty based on the fitting of the angular distributions and different choices for the continuum, as described in the text. Gaussian fits to the E1 distributions for the individual peaks (blue and purple) and their sum (red) are shown. The green lines are the strength distributions obtained with the HF-RPA calculations using the KDE0v1 interaction, smeared to more closely represent the data as discussed in the text. The orange lines are the HF-RPA strength distributions without smearing and with the strength scaled to fit on the figure.

Table III. Parameters for energy moments obtained for isoscalar multipoles in ^{44}Ca are listed. The moments from the KDE0v1 calculation results are over the experimental energy range 9≤Ex≤40 MeV.

	Moments			
	$E0$		$E1$	$E2$
	Exp.	KDE0v1		
m_1 (Frac. EWSR)	$0.75 \pm .11$	0.94	$0.48 \pm .19/.18$	$0.77 \pm .14$
m_1/m_0(MeV)	$19.50 \pm .35/.33$	19.55	$25.97 \pm 1.71/1.59$	$17.21 \pm .48$
rms width (MeV)	$5.84 \pm .86/.73$	5.01	$8.55 \pm 1.03/.84$	$5.06 \pm 1.28/1.15$
$\sqrt{m_3/m_1}$ (MeV)	$21.78 \pm .84/.72$	21.28	$30.11 \pm 2.09/1.84$	$19.01 \pm 1.02/.95$
$\sqrt{m_1/m_{-1}}$ (MeV)	$18.73 \pm .29$	18.97	$24.05 \pm 1.49/1.45$	$16.71 \pm .41$

Table IV. Parameters obtained for Gaussian fits for isoscalar multipoles in ^{44}Ca are listed.

	Gaussian fits		
	$E1$ peak 1	$E1$ peak 2	$E2$
Centroids (MeV)	$16.46 \pm 1.39/1.55$	$34.92 \pm 1.57/1.34$	17.13±.11
FWHM (MeV)	$4.86 \pm 2.12/2.39$	$16.34 \pm 2.26/2.31$	9.40±.14
Frac. EWSR	0.07	0.53	0.68

Table V. Parameters obtained for energy moments from the KDE0v1 calculation are listed. The results are over the experimental energy ranges (E1 low range: $9 \leq E_x \leq 20$ MeV, E1 high range: $20 \leq E_x \leq 40$ MeV, and E2: $9 \leq E_x \leq 40$ MeV)

	KDE0v1		
	$E1$ low range	$E1$ high range	E2
m_1/m_0 (MeV)	14.37	29.16	16.71
rms width (MeV)	3.42	5.01	4.89
m_1 (Frac. EWSR)	0.15	0.58	0.92

In addition to the experimental uncertainties indicated in the tables for the EWSR, a variation of optical parameters has been shown to change the DWBA cross-sections [24] by 10-15%.

A. E0 Strength

In ^{44}Ca, 75% of the E0 EWSR was identified. The strength distribution is similar to those observed in the other nuclei of this mass region ($40 \leq A \leq 90$) [2,8,25,26]. The shape is asymmetric with a large tailing on the high energy side which extends to 35 MeV. The shape is similar to the E0 strength in ^{48}Ca. The tailing in other nuclei of this region typically extends to 30 MeV. The theoretical prediction for the strength distribution appears to fit the rise of the peak on the low-energy side of the experimental distribution well and has two narrow components separated by about 4 MeV. There is some tailing to the higher energy theoretical component, and it is similar to the tailing seen in the experimental peak.

Figure 4 shows the energy moments obtained for ^{44}Ca along with the published results for ^{40}Ca [8] and ^{48}Ca [2] along with the theoretical predictions from the fully self-consistent calculations with KDE0v1. The theoretical predictions for the scaling energy $\left(\sqrt{\frac{m_3}{m_1}}\right)$, centroid energy $\left(\frac{m_1}{m_0}\right)$, and constrained energy $\left(\sqrt{\frac{m_1}{m_{-1}}}\right)$ are all in agreement within experimental errors with the experimental energies for ^{44}Ca.

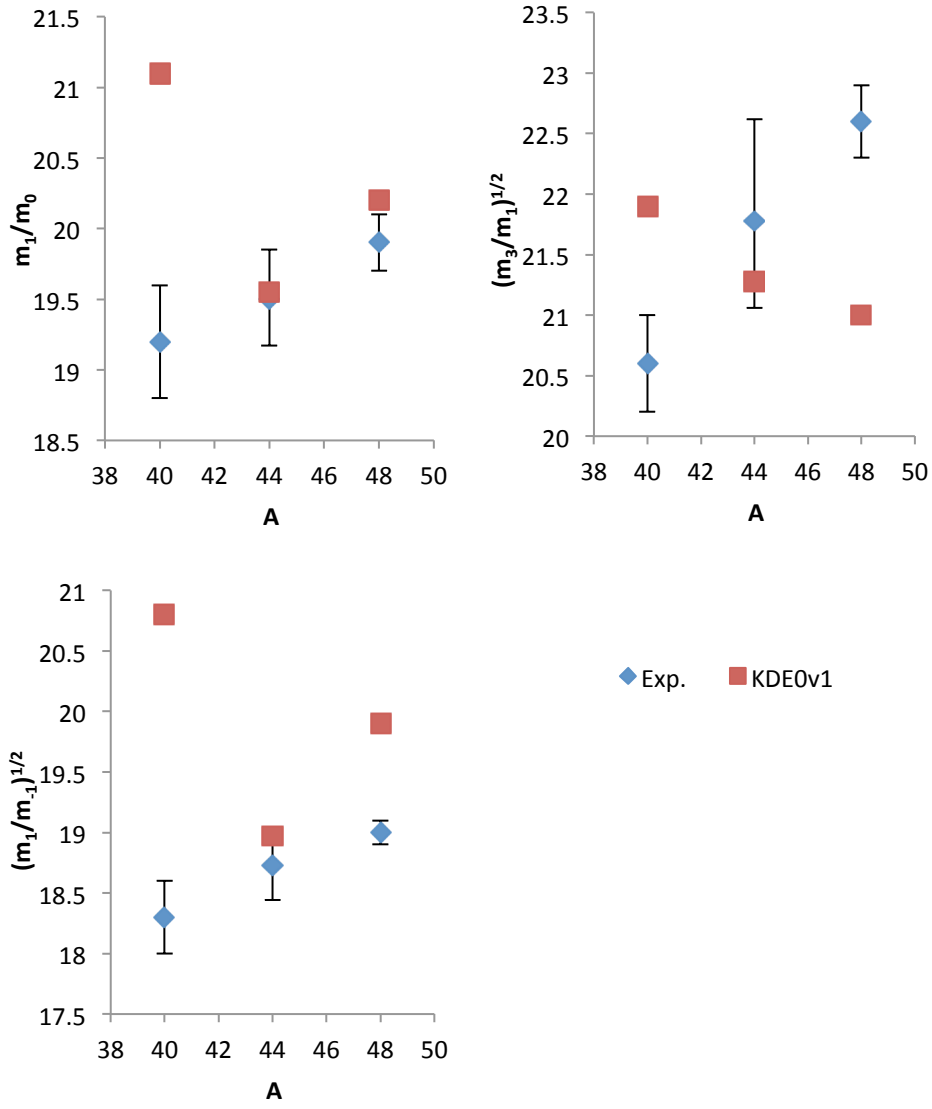

Figure 4. Experimental results for ISGMR energies in ^{40}Ca [8], ^{44}Ca (present work), and ^{48}Ca [2] (blue diamonds) are compared with theoretical predictions. The results of fully self-consistent HF-RPA calculations [4] with KDE0v1 [6] are shown using the experimental excitation energy range (E=9.5-40 MeV) (red squares).

There have been a number of attempts to deduce K_τ, the symmetry term from the Leptodermous expansion,

$$K_A = K_{NM} + K_S A^{-\frac{1}{3}} + K_\tau \delta^2 + \frac{K_{Coul} Z^2}{A^{\frac{4}{3}}} + \cdots \qquad (1)$$

using values of K_A obtained from the measured monopole energies in different nuclei within an isotopic chain, such as Cd (K_τ = -555±75 MeV) [27] and Sn (K_τ = -550±100 MeV) [3,28]. In Ref. [29], analysis of GMR data for Sn and Sm nuclei from 120 MeV inelastic α-scattering, along with data for ^{208}Pb and ^{24}Mg, resulted in a value for the symmetry term, K_τ = -320±184 MeV. Within an isotopic chain, the nuclear charge is fixed, and therefore the neutron-proton asymmetry (N-Z)/A increases when A increases. Although the surface and Coulomb contributions become a little less negative with increasing A, the negative increase of the symmetry contribution dominates. The variations of K_τ from Skyrme interactions are K_τ = -400±100 MeV and effective relativistic mean field Lagrangians are K_τ = -620±180 MeV [30]. In Figure 4, it is apparent that in the Ca isotopes the monopole energy, and by extension K_A, is rising instead of falling with A. This behavior is shown in Figure 5 with a calculation of K_A from Leptodermous expansion for K_{NM} = 200 MeV and K_τ = 582 MeV which reproduces the data. This suggests that in the Ca isotopes it is unlikely that calculations with common effective interactions will reproduce the mass dependence of the GMR energies (as found by Anders et al. [4]) without the addition of nuclear structure effects.

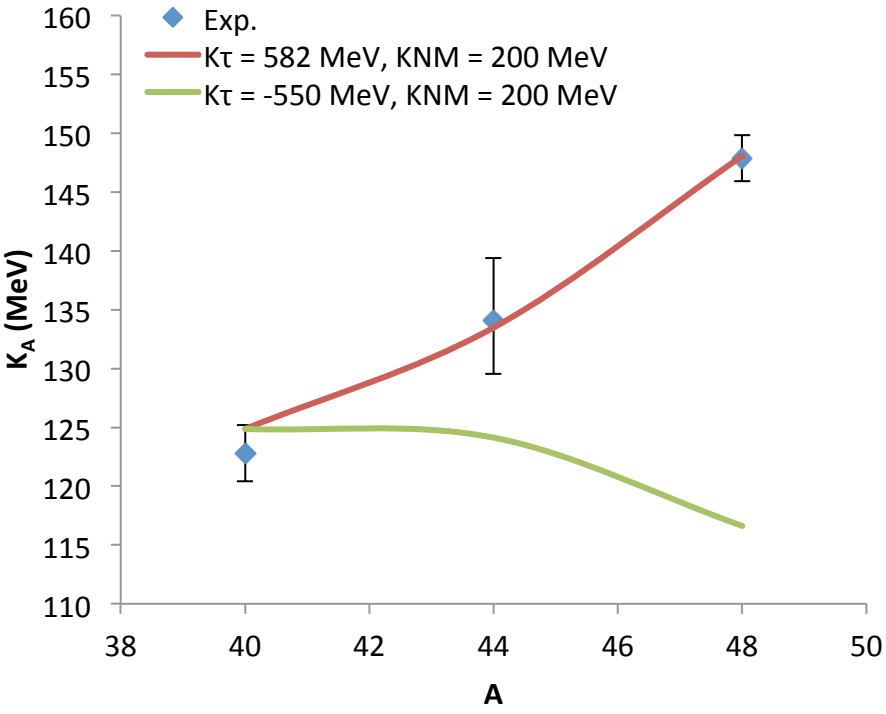

Figure 5. Values of K_A from the scaling energy $\sqrt{(m_3/m_1)}$ for the Ca isotopes are plotted against A. A fit to the data (red line) using the Leptodermous expansion with the parameters indicated is shown. The green line is shown as a reference and is also from the Leptodermous expansion but with K_τ=-550 MeV.

B. E1 Strength

In ^{44}Ca, $48\pm^{19}_{18}\%$ of the E1 strength was identified. This is much less than the E1 strength $(137 \pm 20\%)$ identified for ^{48}Ca [2] but is similar to the amount identified in ^{40}Ca ($62\pm^{10}_{20}\%$) [8]. The strength is distributed in low and high energy components. The E1 strength is particularly sensitive to the choice of continuum because of the low ratio of peak-to-continuum at the higher end of the energy range where the majority of the E1 strength is found. This sensitivity has been observed in ^{48}Ca, ^{40}Ca and in other nuclei. [25,26]. For ^{40}Ca, changes in the continuum choice resulted in shifts of m_1/m_0 of up to 2.5 MeV and sum-rule variation from 28-

94%. The centroid energy m_1/m_0 for ^{40}Ca is 23.36±0.70 MeV, which is about 3 MeV less than the energy observed in ^{44}Ca. The low peak component observed in ^{44}Ca is narrow and is fit with a Gaussian with centroid energy of $16.51\pm^{.78}_{.74}$ MeV. It contains about 7% of the E1 strength. The Gaussian fit to the high peak is much broader, extending well beyond the E_x=40 MeV cut off of the experiment. It has a centroid energy of $35.37\pm^{.67}_{.56}$ MeV, and its strength corresponds to 53% of the EWSR. Much more strength was identified in ^{48}Ca, but it has a similar ≈1:8 ratio of the strength in the low peak to that in the high peak. The energy of the low component is in agreement with that found for ^{48}Ca ($16.69\pm^{.39}_{.33}$ MeV). The energy of the high components of the E1 strength in both nuclei ($37.28\pm^{.71}_{1.98}$ MeV for ^{48}Ca) are also in agreement within experimental error. The E1 strength that results from the HF-RPA calculation with KDE0v1 interaction does not fit the experimental distribution well, and it has several components. The majority of the strength is in a peak located at 29.16 MeV, which is lower than the experimental high energy component by ≈7 MeV. The majority of the strength in the low energy range ($9\leq E_x\leq 20$ MeV) appears in a broad peak located at ≈13 MeV, while the centroid is a bit higher at 14.37 MeV, which is ≈2 MeV less than the experimental centroid.

C. E2 Strength

A majority of the E2 strength ($77 \pm 14\%$) was identified in the experimental data. The theoretical prediction of the E2 strength over the range 9 to 40 MeV shows approximately 20% more strength than the experimental distribution. The predicted strength is in a single peak with a centroid of 16.71 MeV, which is close to the experimental centroid ($17.21 \pm .48$ MeV). The E2

strength in ^{48}Ca was roughly Gaussian with the exception of some strength found in a tail extending to 35 MeV. The ^{44}Ca centroid is slightly lower than that for ^{40}Ca (17.84±0.43 MeV).

VI. SUMMARY

Close to 70% of the E0 and E2 strength was identified, and nearly half of the E1 strength has been located between 9 and 40 MeV in ^{44}Ca. The E1 strength distribution obtained for the GR peak was sensitive to the continuum choice. The E0 distribution is asymmetric with a tail at higher excitation that is similar to that found in ^{48}Ca. The microscopic calculation with KDE0v1 interaction predicts energies for E0 that are in good agreement with the experimental values. It may be interesting to extend the calculations beyond RPA to include coupling to more complex configurations. The analysis done with collective-model based transition densities in the DWBA calculation may result in overestimation of the EWSR and shifts of the centroid energy [31], so it may be interesting to do the analysis with microscopic transition densities instead. The GMR energy moments for ^{40,44,48}Ca are consistent with an increasing energy with mass, contrary to what would be expected with a negative K_τ. However, while it is clear the GMR energy moments in ^{48}Ca are higher than those in ^{40}Ca, the uncertainties are such that we can only say those in ^{44}Ca do not contradict this trend. Thus in the Ca isotopes it seems unlikely that calculations with common effective interactions will reproduce the mass dependence of the GMR energies without the addition of nuclear structure effects.

ACKNOWLEDGMENTS

This work was supported, in part, by the U.S. Department of Energy under Grant No. DE-FG03-93ER40773.

REFERENCES

[1] D. H. Youngblood, Y. -W. Lui, and H. L. Clark, Physical Review C **55**, 2811 (1997).

[2] Y. -W. Lui, D. H. Youngblood, S. Shlomo, X. Chen, Y. Tokimoto, M. Anders, and J. Button, Phys. Rev. C **83**, 044327 (2011).

[3] T. Li, U. Garg, Y. Liu, R. Marks, B. Nayak, P. M. Rao, M. Fujiwara, H. Hashimoto, K. Nakanishi, and S. Okumura, Phys. Rev. C **81**, 034309 (2010).

[4] M. R. Anders, S. Shlomo, T. Sil, D. H. Youngblood, and Y. -W. Lui, Phys. Rev. C **87**, 024303 (2013).

[5] P. - G. Reinhardt, Ann. Phys. (Leipzig) **1**, 632 (1992).

[6] B. K. Agrawal, S. Shlomo, and V. K. Au, Phys. Rev. C **72**, 014310 (2005).

[7] D. H. Youngblood, Y. -W. Lui, and H. L. Clark, Phys. Rev. C **65**, 034302 (2002).

[8] D. H. Youngblood, Y. -W. Lui, and H. L. Clark, Phys. Rev. C **63**, 067301 (2001).

[9] D. M. Pringle, W. N. Catford, J. S. Winfield, D. G. Lewis, N. A. Jelley, K. W. Allen, and J. H. Coupland, Nucl. Instrum. Methods A **245**, 230 (1986).

[10] J. S. Winfield, D. M. Pringle, W. N. Catford, D. G. Lewis, N. A. Jelley, and K. W. Allen, Nucl. Instrum. Methods A **251**, 297 (1986).

[11] D. H. Youngblood, Y. -W. Lui, H. L. Clark, P. Oliver, and G. Simler, Nucl. Instrum. Methods A **361**, 539 (1995).

[12] G. R. Satchler and D. T. Khoa, Phys. Rev. C **55**, 285 (1997).

[13] M. Rhoades-Brown, S. Pieper, and M. Macfarlane, *in Argonne National Laboratory Report* (Argonne National Laboratory, Argonne, 1978).

[14] G. Fricke, C. Bernhardt, K. Heilig, L. A. Schaller, L. Schellenberg, E. B. Shera, and C. W. De Jager, At. Data Nucl. Data Tables **60**, 177 (1995).

[15] L. Ray, W. Rory Coker, and G. W. Hoffmann, Phys. Rev. C **18**, 2641 (1978).

[16] G. R. Satchler, Nucl. Phys. A **472**, 215 (1987).

[17] H. L. Clark, Y. -W. Lui, and D. H. Youngblood, Phys. Rev. C **57**, 2887 (1998).

[18] J. Button, Y. -W. Lui, D. H. Youngblood, X. Chen, G. Bonasera, and S. Shlomo, Phys. Rev. C **94**, 034315 (2016).

[19] S. Shlomo, V. M. Kolomietz, and G. Colò, Eur. Phys. J. A **30**, 23 (2006).

[20] A. Bohr and B. R. Mottelson, *Nuclear Structure* (W.A. Benjamin, New York, 1975), Vol. 2.

[21] D. H. Youngblood, Y. -W. Lui, J. Button, G. Bonasera, and S. Shlomo, Phys. Rev. C **92**, 014318 (2015).

[22] P. Stevenson, P. Goddard, J. Stone, and M. Dutra, arXiv preprint arXiv:1210.1592 (2012).

[23] M. Dutra, O. Lourenço, J. S. Martins, A. Delfino, J. R. Stone, and P. Stevenson, Physical Review C **85**, 035201 (2012).

[24] Krishichayan, X. Chen, Y. -W Lui, J. Button, and D. H. Youngblood, Physical Review C **81**, 044612 (2010).

[25] Y. -W. Lui, D. H. Youngblood, H. L. Clark, Y. Tokimoto, and B. John, Phys. Rev. C **73**, 014314 (2006).

[26] Y. Tokimoto, Y. -W. Lui, H. L. Clark, B. John, X. Chen, and D. H. Youngblood, Phys. Rev. C **74**, 044308 (2006).

[27] D. Patel, U. Garg, M. Fujiwara, H. Akimune, G. Berg, M. Harakeh, M. Itoh, T. Kawabata, K. Kawase, and B. Nayak, Phys. Lett. B **718**, 447 (2012).

[28] T. Li, U. Garg, Y. Liu, R. Marks, B. Nayak, P. M. Rao, M. Fujiwara, H. Hashimoto, K. Kawase, and K. Nakanishi, Phys. Rev. Lett. **99**, 162503 (2007).

[29] M. M. Sharma, W. T. A. Borghols, S. Brandenburg, S. Crona, A. Van der Woude, and M. N. Harakeh, Phys. Rev. C **38**, 2562 (1988).

[30] G. Colò, U. Garg, and H. Sagawa, Eur. Phys. J. A **50**, 1 (2014).

[31] A. Kolomiets, O. Pochivalov, and S. Shlomo, Phys. Rev. C **61**, 034312 (2000).